Theoretical Notes

Note 228

February 1973

Nonlinear Electromagnetic Fields Within a Cylindrical Cavity Excited by Ionizing Radiation*

D. E. Merewether
W. A. Radasky
Mission Research Corporation
Albuquerque, New Mexico 87108

Abstract

A numerical solution is provided that may be used to predict the electromagnetic field within a partially evacuated cylindrical cavity excited by a pulse of ionizing radiation. Several examples are given to illustrate the pressure dependence of the nonlinear response and to acquaint the reader with principal characteristics of this response.

*This work was supported by the U. S. Army Safeguard System Command, under contract DAHC60-72-C-0038.

Table of Contents

Introduction

Transient sources of ionizing radiation produce electromagnetic fields within a test vessel. These fields can sometimes couple currents into an instrumentation cable that exceed the the desired or expected signal, thereby endangering the experiment or even the equipment itself.

Being able to predict the radiation-induced internal electromagnetic pulses (IEMP) can help the experimenter design test vessels and experiments to minimize the potential effect on the experiment.

Earlier papers have estimated the fields in small cavities (quasi-static fields) [1] and the fields in large cavities filled with homogeneous time-invarient media [2,3]. This paper provides a numerical solution to the problem of preeicting fields in a reasonably large cavity filled with air under partial pressure. This type of solution is most appropriate for treating the nonlinear, inhomogeneous, time-dependent air media.

Examples are given to illustrate how the air pressure influences the conductivity within a test vessel and how this conductivity influences the electromagnetic field within the vessel.

Formulation

The problem to be addressed is to determine the total electromagnetic field within a cylindrical cavity driven by ionizing radiation (Figure 1). It is assumed that the walls are metallic and that the cylinder contains air under a partial vacuum.

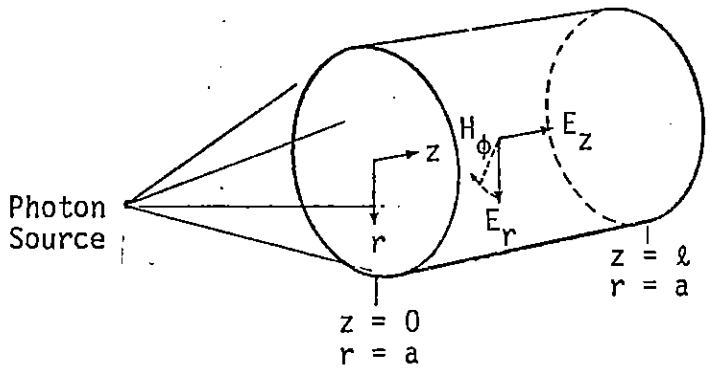

Figure 1. Radiation Excited Cavity

The electromagnetic field within the cylinder satisfies Maxwell's equations,

$$\nabla \times \vec{e} = -\mu_o \frac{\partial \vec{h}}{\partial t} \tag{1}$$

$$\nabla \times \vec{h} = \vec{J}_s + \sigma \vec{e} + \varepsilon_o \frac{\partial \vec{e}}{\partial t} \quad , \tag{2}$$

where $\vec{e}$ and $\vec{h}$ are the total electric and magnetic fields within the cavity and ε_o and μ_o are the free space permittivity, $\varepsilon_o = 10^{-9}/36\pi$ f/m and $\mu_o = 4\pi \times 10^{-7}$ h/m. σ is the air conductivity in mhos per meter, $\sigma = \sigma(\vec{e},z,r,t)$, a complex function of time, space and electric field intensity. $\vec{J}_s$ is the radiation induced conventional current in amps/meter^2. For the problem at hand, we shall assume that the source currents possess azimuthal symmetry such that there is no ϕ dependence of any field component and the curl equations (1) and (2) reduce to:

$$\left(\frac{\partial e_r}{\partial z} - \frac{\partial e_z}{\partial r}\right) = -\mu_o \frac{\partial h_\phi}{\partial z} \tag{3}$$

$$\left(-\frac{\partial h_\phi}{\partial z}\right) = j_r + \sigma e_r + \varepsilon_o \frac{\partial e_r}{\partial t} \tag{4}$$

$$\left(\frac{h_\phi}{r} + \frac{\partial h_\phi}{\partial r}\right) = j_z + \sigma e_z + \varepsilon_o \frac{\partial e_z}{\partial t} \tag{5}$$

The nonzero components of the scattered field satisfy these equations and are subject to the boundary conditions, $e_z = 0$ at $r = a$ and $e_r = 0$ for $z = 0$ and $z = \ell$.

This system of simultaneous partial differential equations (3)-(5) is easily solved using finite difference techniques to yield the fields within the vessel.

Numerical Solution of Maxwell's Equations

The formulation of the difference equation follows that devised by Yee [4] and previously used to study the current distribution on scatterers in various inhomogeneous media [5]. The resultant difference equations are

$$h_\phi^{n+1}(i,j) = h_\phi^n (i,j) + \frac{\Delta t}{\mu_o \Delta r}\left[e_z^n (i,j+1) - e_z^n (i,j)\right] - \frac{\Delta t}{\mu_o \Delta z}\left[e_r^n (i+1,j) - e_r^n (i,j)\right]$$

for $1 \le j \le j_{can}$ and $1 \le i \le i_{can}$. (6)

$$e_r^{n+1}(i+1,j) = \left\{e_r^n (i+1,j) \times \left(1 - \frac{\Delta t\, \sigma_r^{n+1/2}(i+1,j)}{2\varepsilon_o}\right) - j_r^{n+1/2}(i+1,j)\left(\frac{\Delta t}{\varepsilon_o}\right) - \left[h_\phi^{n+1}(i+1,j) - h_\phi^{n+1}(i,j)\right]\left(\frac{\Delta t}{\varepsilon_o \Delta z}\right)\right\} \Big/ \left\{1 + \frac{\Delta t\, \sigma_r^{n+1/2}(i+1,j)}{2\varepsilon_o}\right\}$$

for $1 \le j \le j_{can}$ and $1 \le i \le \left(i_{can} - 1\right)$. (7)

$$e_z^{n+1}(i,j+1) = \left\{ e_z^n(i,j+1) \times \left(1 - \frac{\Delta t\, \sigma_z^{n+1/2}(i,j+1)}{2\varepsilon_o} \right) - j_z^{n+1/2}(i,j+1) \left(\frac{\Delta t}{\varepsilon_o} \right) + \left[h_\phi^{n+1}(i,j+1) - h_\phi^{n+1}(i,j) \right] \left(\frac{\Delta t}{\varepsilon_o \Delta r} \right) + \left[h_\phi^{n+1}(i,j+1) + h_\phi^{n+1}(i,j) \right] \left(\frac{\Delta t}{\varepsilon_o 2j\Delta r} \right) \right\} \Bigg/ \left\{ 1 + \frac{\Delta t\, \sigma_z^{n+1/2}(i,j+1)}{2\varepsilon_o} \right\}$$

for $1 \le j \le (j_{can}-1)$ and $1 \le i \le i_{can}$, (8)

where

$$h_\phi^n(i,j) = h_\phi(t,r,z) \quad \begin{vmatrix} t = n\Delta t \\ z = (i-1)\Delta z \\ r = (j-.5)\Delta r \end{vmatrix} \tag{9}$$

$$e_r^n(i,j) = e_r(t,r,z) \quad \begin{vmatrix} t = (n+.5)\Delta t \\ z = (i-1.5)\Delta z \\ r = (j-.5)\Delta r \end{vmatrix} \tag{10}$$

$$e_z^n(i,j) = e_z(t,r,z) \quad \begin{vmatrix} t = (n+.5)\Delta t \\ z = (i-1)\Delta z \\ r = (j-1)\Delta r \end{vmatrix} \tag{11}$$

The source functions and conductivities are evaluated at time halfway between the old and new values of e; that is

$$\begin{aligned} j_r^{n+1/2}(i,j) &= j_r(t,r,z) \\ \sigma_r^{n+1/2}(i,j) &= \sigma(t,r,z) \end{aligned} \quad \begin{vmatrix} t = (n+1)\Delta t \\ z = (i-1.5)\Delta z \\ r = (j-.5)\Delta r \end{vmatrix} \tag{12}$$

$$\begin{aligned} j_z^{n+1/2}(i,j) &= j_z(t,r,z) \\ \sigma_z^{n+1/2}(i,j) &= \sigma(t,r,z) \end{aligned} \quad \begin{vmatrix} t = (n+1)\Delta t \\ z = (i-1)\Delta z \\ r = (j-1)\Delta r \end{vmatrix} \tag{13}$$

The conductivity σ is just a scalar function of position. The difference between σ_r and σ_z is that value of σ is computed at a slightly different spatial location. The values of Δr and Δz are related to the length and radius of the cavity by

$$\Delta z = \ell \Big/ \left(i_{can} - 1\right)$$

$$\Delta r = a/j_{can} \ ,$$

where i_{can} and j_{can} are to be chosen such that Δr and Δz are each less than 0.2λ, where λ is the free space wavelength of the highest frequency component of interest.

The boundary conditions are applied as

$$e_z(t,r,z)\Big|_{r=a} = 0 \rightarrow e_z^n\left(i,j_{can}\right) + 1 = 0 \quad \text{for all } i,n \ , \tag{14}$$

$$e_r(t,r,z)\Big|_{z=0} = 0 \rightarrow e_r^n(1,j) = -e_r^n(2,j) \quad \text{for all } j,n \ , \tag{15}$$

and

$$e_r(t,r,z)\Big|_{z=\ell} = 0 \rightarrow e_r^n\left(i_{can}+1,j\right) = -e_r^n\left(i_{can},j\right) \quad \text{for all } j,n \ . \tag{16}$$

The formal solution is now complete. The reader should refer to References 4 and 5 for a discussion of the finite difference techniques used here. However, a few comments are in order. Note that h_ϕ^{n+1} is computed from e_r^n and e_z^n, while e_r^{n+1} and e_z^{n+1} is computed from h_ϕ^{n+1}. For a system initially at rest, $e_r = e_z = h_\phi = 0$ at $t = 0$, the solution proceeds by computing e_r^1 and e_z^1 can then be used to compute h_ϕ^2. The solution proceeds sequentially to any desired time.

Calculation of the Source Current Density

The source of the cavity fields is the radiation-induced current

$$\vec{J}_s = -q\, n_p \vec{v} \ . \tag{17}$$

Here q is the charge on an electron (1.6×10^{-19} coul), and n_p is the density of primary electrons (electrons/m^3) traveling at velocity, v (meters/sec).

For high energy photon sources $\left(\vec{E}_\gamma > .25 \text{ MeV}\right)$ electron production results primarily from the Compton effect so that the electrons are ejected with a forward velocity component $\vec{v}_f$ on the order of the velocity of light. The production rate of these primary electrons is proportional to the ionization rate [6],

$$\dot{n}_p\ (\vec{r};t) = \frac{\dot{\gamma}(\vec{r},t)}{\vec{E}_\gamma R_\gamma(\vec{E}_\gamma)} \qquad (18)$$

Here $\dot{\gamma}$ is the photon flux rate in MeV $m^{-2}sec^{-1}$. $\vec{E}_\gamma$ is the average energy of the gamma flux and R_γ is the mean range of a photon (meters). For an isotropic source of gamma rays the current density at a particular point in space and time is determined by adding the contributions of all the primary electrons made closer to the source at the appropriate time. Thus,

$$\vec{J}_s(r,t) = \frac{-qv_f\vec{a}_r}{4\pi r^2} \int_o^t dt' \int_o^r dr'\ \dot{n}_p(r',t')\ 4\pi r'^2$$
$$\times\ u\left(R_{ef} - (r-r')\right)\ \ \delta\left(r-r'-v_f(t-t')\right) \qquad . \qquad (19)$$

Here R_{ef} is the mean forward range of an electron; $u(x)$ and $\delta(x)$ are the normally defined Heaviside step and Dirac delta functions, respectively.

In writing (19) for simplicity it was assumed that the electrons all travel with their initial velocity v_f throughout their mean forward range, R_{ef}, then stop abruptly. In evaluating this integral we shall ignore atmospheric attenuation of the gamma flux over the distances involved here. The $\dot{n}_p$ has the form

$$\dot{n}_p\ (r',t') = f(t'-r'/c)/r'^2 \qquad . \qquad (20)$$

Then if $r > R_{ef}$ the integral is just

$$\vec{J}_s(r,t) = -q\,\frac{v_f\vec{a}_r}{r^2} \int_o^{\frac{R_{ef}}{v_f}} f\left(t - \frac{r}{c} - t''\left(1 - \frac{v_f}{c}\right)\right) dt'' \qquad . \qquad (21)$$

For Compton electrons produced by high energy photons (0.25 MeV $\leq \vec{E}_\gamma \leq$ 5 MeV) the maximum delay factor (in air at sea level) is

$$\frac{R_{ef}}{v_f}\left(1 - \frac{v_f}{c}\right)\Big|_{max} \simeq .5 \text{ nsec} \qquad . \quad (22)$$

The effect of this delay is to average the gamma flux over the time interval involved and to delay the current pulse behind the gamma pulse by this same amount [7]. We shall ignore this difference; then the integral is simply

$$\vec{j}_s(r,t) = -q\,\frac{v_f \vec{a}_r}{r^2}\, f\,(t-r/c)\left(\frac{R_{ef}}{v_f}\right) \qquad . \quad (23)$$

Reintroducing the definitions of f and $\dot{n}_p$ we have

$$\vec{j}_s(r,t) = -q\,\frac{\dot{\gamma}(r,t)}{\vec{E}_\gamma}\,\frac{R_{ef}}{R_\gamma}\,\vec{a}_r \quad ,$$

and the proportionality constant $f_{\gamma j}(\vec{E})$, (Figure 2), defined by

$$f_{\gamma j} = j_s \Big/ \dot{\gamma} \qquad (25)$$

does not depend upon the air pressure in the partially evacuated cylinder, since both R_{ef} and R_γ are inversely proportional to pressure and only their ratio appears in (24). The $\dot{\gamma}$ used here was assumed to be in units of MeV $m^{-2}sec^{-1}$; however, $f_{j\gamma}$ is also given for cases where $\dot{\gamma}$ is given in roentgen/sec. The mean free path of an electron in air varies inversely with relative air density $\left[R_{ef} \sim 1 \Big/ \left(\rho/\rho_o\right)\right]$. For most evacuated canisters the range of integration in (21) exceeds the transit time of the test vessel. Note, however, that electrons are made within the metal walls of the vessel maintaining about the same proportionality (25) between electron flux and gamma flux.

We have also tacitly ignored the effect of the fields created by the motion of the primary electrons on their own flight. For reasonably sized test vessels the fields are not large enough to influence the primary electrons during their transit time across the cavity.

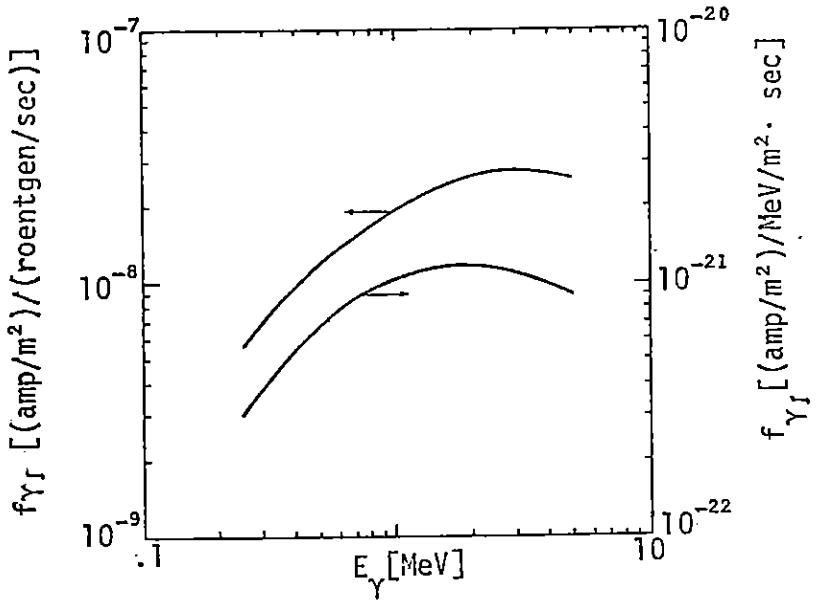

Figure 2. Energy dependent proportionality constant relating current density to photon flux.

Calculation of the Air Conductivity

The air conductivity, $\sigma = \sigma\left(|\vec{e}|\ \rho_r\right)$ is defined as

$$\sigma = q\ [n_e \mu_e + \left(n_- + n_+\right)\ \mu_i] \tag{26}$$

Here n_e is the number density of secondary electrons [m^{-3}], n_- and n_+ are the number density of negative and positive ions [m^{-3}], and μ_e and μ_i are the electron and ion mobilities [m^2/volt·sec]. For a relative air density of 1, $\mu_i = 2.5\times10^{-4} m^2$/volt·sec while μ_e varies between 10^2 and 10^4 times as large as the ion mobility, the electron density is the major contributor to conductivity. When the ion conductivity is relevant, it may be added but this procedure will not be discussed here. Equation (26) simplifies to

$$\sigma\left(|\vec{e}|,\ \rho_r\right) = q\ n_e\left(|\vec{e}|,\ \rho_r\right)\ \mu_e\left(|\vec{e}|,\ \rho_r\right)$$

Only two variables are now required: the conduction electron density and mobility.

The source of the secondary electrons is the magnitude of the ionization rate function, $\dot{\gamma}(z,r,t)$, times a conversion factor, $K(\rho_r)$. As $\dot{\vec{\gamma}}$ is expressed in roentgens/sec and 1 roentgen is equivalent to 1.61×10^{12} ion pairs/g air, we may define an electron source function, Q, with units of [electrons/m^3·sec] as

$$Q(z,r,t,\rho_r) = K(\rho_r)\,\dot{\gamma}(z,r,t) \quad , \quad (28)$$

with

$$K(\rho_r) = [1.61\times10^{12}\,(\text{electrons/g air})/\text{roentgen}] \times \left[\frac{1.225\times10^{3}\,g}{m^3}\right]\rho_r, \text{ and} \quad (29)$$

$$K(\rho_r) = 1.972\times10^{15}\,\rho_r[\text{electrons/m}^3)/\text{roentgen}] \quad . \quad (30)$$

With the electron source function defined, it is now possible at a fixed position (r,z = constant) and for a constant air density (ρ_r = constant) to define the electron density as a function of time (t) and electric field strength, $|\vec{e}|$. The equation representing the conduction electron density generation is

$$\frac{dn_e(r,z,t)}{dt} + \alpha_e\left(|\vec{e}|,\rho_r\right) n_e(r,z,t) = Q(z,r,t,\rho_r) + G\left(|\vec{e}|,\rho_r\right) n_e(r,z,t) \quad , \quad (31)$$

where n_e is the number density of conduction electrons [m^{-3}], Q is the electron source function, α_e is the attachment rate of electrons to O_2 [sec^{-1}], and G is the electron avalanching or "breakdown" effect rate [sec^{-1}]. Simplifying equation (31) to consider a fixed position and air density,

$$\frac{dn_e(t)}{dt} + \left[\alpha_e\left(|\vec{e}|\right) - G\left(|\vec{e}|\right)\right] n_e(t) = Q(t) \quad . \quad (32)$$

To solve equation (32) numerically the following differenced solution is employed with analytical fits to the measured attachment and avalanche rates (Figure 3):

$$n_e^{n+1/2} = n_e^{n-1/2}\, e^{-N_e} + \left(1 - e^{-N_e}\right)\frac{Q + Gn_e}{\alpha_e} \quad , \quad (33)$$

with

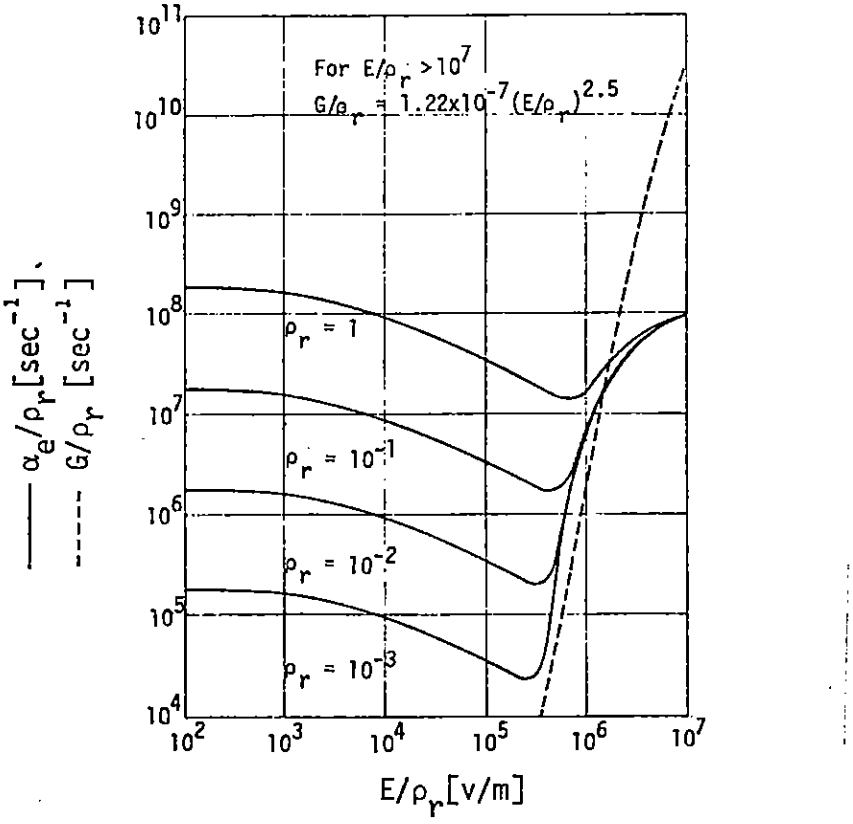

Figure 3. Electron attachment and avalanche coefficients for dry air.

$$N_e = \alpha_e^n \Delta t \quad . \quad (34)$$

With the calculation of the conduction (or secondary) electron density, only the electron mobility remains to be considered. The analytical fits to the measured data used in this analysis were devised by Longmire and Longley [8] (Figure 4).

The electron mobility can be evaluated at the same time and spatial location as the secondary electron density so that

$$\sigma^{n+1/2} = q\, \mu_e^{n+1/2}\, n_e^{n+1/2} \quad . \quad (35)$$

Thus, the conductivity $\sigma\left(|\vec{e}|, \rho_r\right)$ is evaluated for use in equations (1) and (2).

Numerical Examples

The numerical solution presented can be used to predict fields within complex bodies of revolution or fields between coaxial bodies of

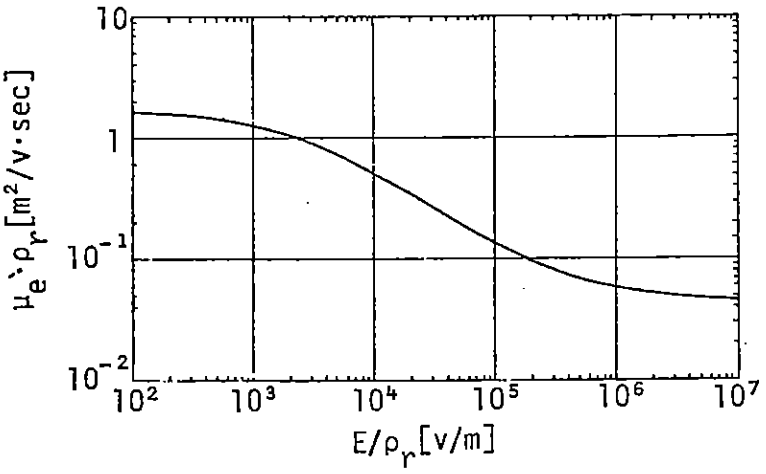

Figure 4. Electron Mobility in Dry Air

revolution. The particular effect selected for study here is the examination of the effects of air pressure on the nonlinear air conductivity and fields within a closed cylinder. Other parametric studies have been done for cylinders filled with linear media [2].

For the numerical examples, a $\sin^2$ pulse approximation with an 18 nsec pulse duration at 1/2 max was selected as the profile of the ionization rate, $\dot{\gamma}$, which corresponds roughly to the pulse shape of the output of the HIFX machine at Harry Diamond Laboratories (HDL). The peak rate of the pulse was varied over three orders of magnitude, 10^8 to 10^{11} roentgen/sec. Four different pressures were examined corresponding to relative air densities of 1, .1, .01 and .001 with respect to the density of air at sea level and a temperature of 20°C. The size of the cylinder selected for study here is two meters long and one meter in diameter, corresponding roughly to the size of a test vessel being used by HDL at the Aurora flash X-ray facility.

For simplicity, it was also assumed here that the photon source was far removed from the test vessel so that there would be essentially no variation in the axially directed source current over the length of the cy cylinder.

For low flux levels, the magnetic field within the cavity is closely approximated by $h_\phi(r,z) = j_z \cdot r/2$ for all z. The electric field

components for $\dot{\gamma} = 10^8$ (roentgen/sec)(E_γ = 1 MeV) illustrate the dependence of the electric field on the nonlinear air conductivity (Figure 5). Each horizontal set of three figures corresponds to a different relative air density, $\rho_r = \rho/\rho_o$. Each individual e_z time history shows the electric field at five axial locations within the can: the ends and three points within the cylinder. Each e_r plot shows only one figure since the e_r component did not change significantly between z/ℓ = .25, .5, and .75. At the ends of the can, the e_r component is zero. The conductivity is also shown at the same five locations that the e_z plots are provided. However, at lower flux levels, the conductivities were essentially the same except at the ends of the cavity.

The case labelled "vacuum" was run with the same computer code except that σ was forced to zero at every grid point within the cylinder. For this case, the e_z component exhibits symmetry about the center of the cavity and the electric field pulse follows the shape of the gamma pulse. For air at atmospheric pressure, the conductivity rises during the gamma pulse, thus allowing secondary electrons to flow over to the walls of the cylinder during the gamma pulse. These electrons cannot flow back at the end of the pulse, however, since the conductivity quickly drops to a very small value. The net effect is to leave some positive charge within the air after the gamma pulse has disappeared. This will decay away with a time constant which is not discernible on the time scale provided.

Since the attachment rate is proportional to the square of the relative air density at low field intensities (Figure 3), the rate of decay for the air conductivity is very slow compared to the time interval shown on Figure 5 (ρ/ρ_o = .1). This slow decay of the electrical conductivity results in a decay of the static fields previously observed at ρ/ρ_o= 1.

For an intense $\dot{\gamma}$ rate of 10^{11} roentgen/sec (Figure 6), the basic character of the electric field pulse is different. The primary effect is due to the large increase in conductivity. For highly conducting media, the fields in a canister look more like the time derivative of the $\dot{\gamma}$ pulse rather than the pulse itself.

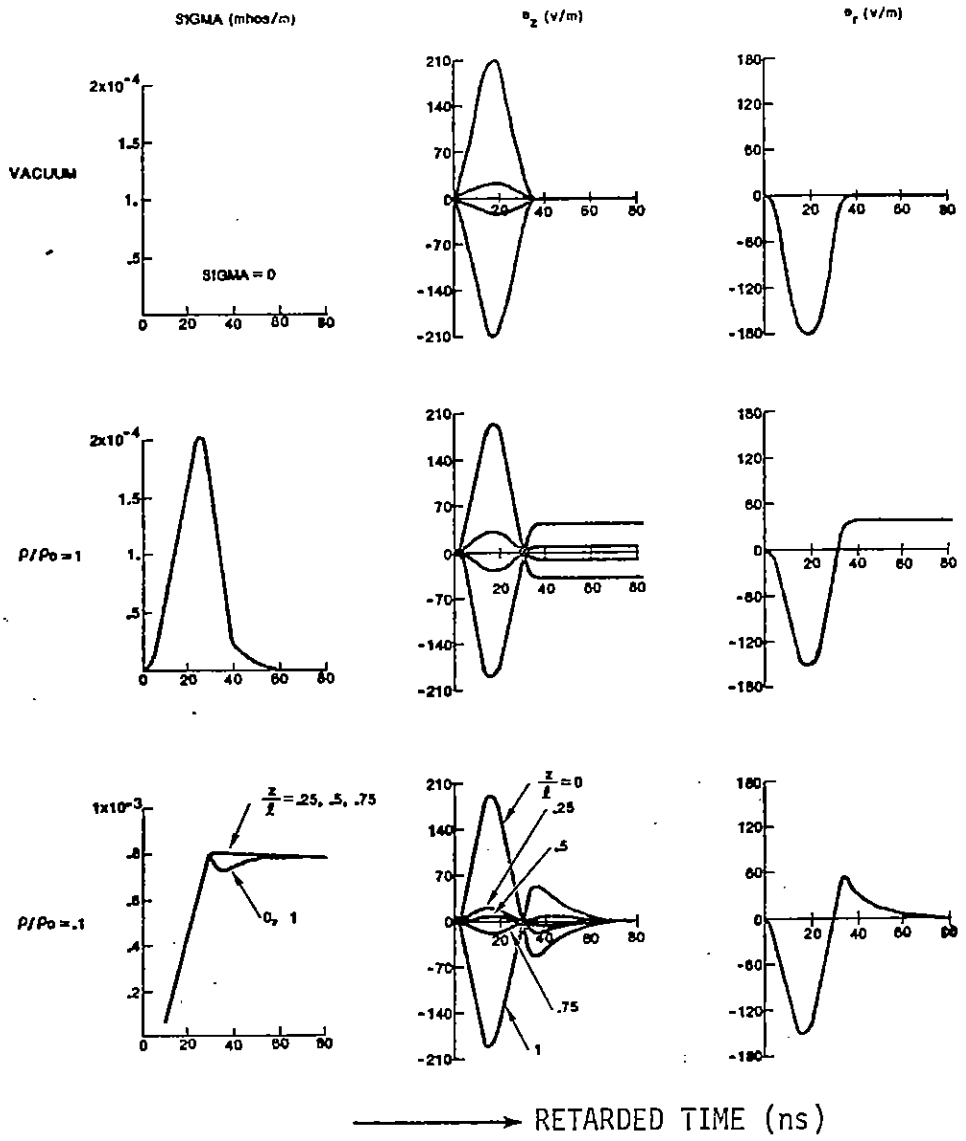

Figure 5. Conductivity and electric fields within a cylindrical cavity (a = .5m, ℓ = 2m) driven by a 1×10^{8} roentgan/sec gamma flux, E_γ = 1 MeV.

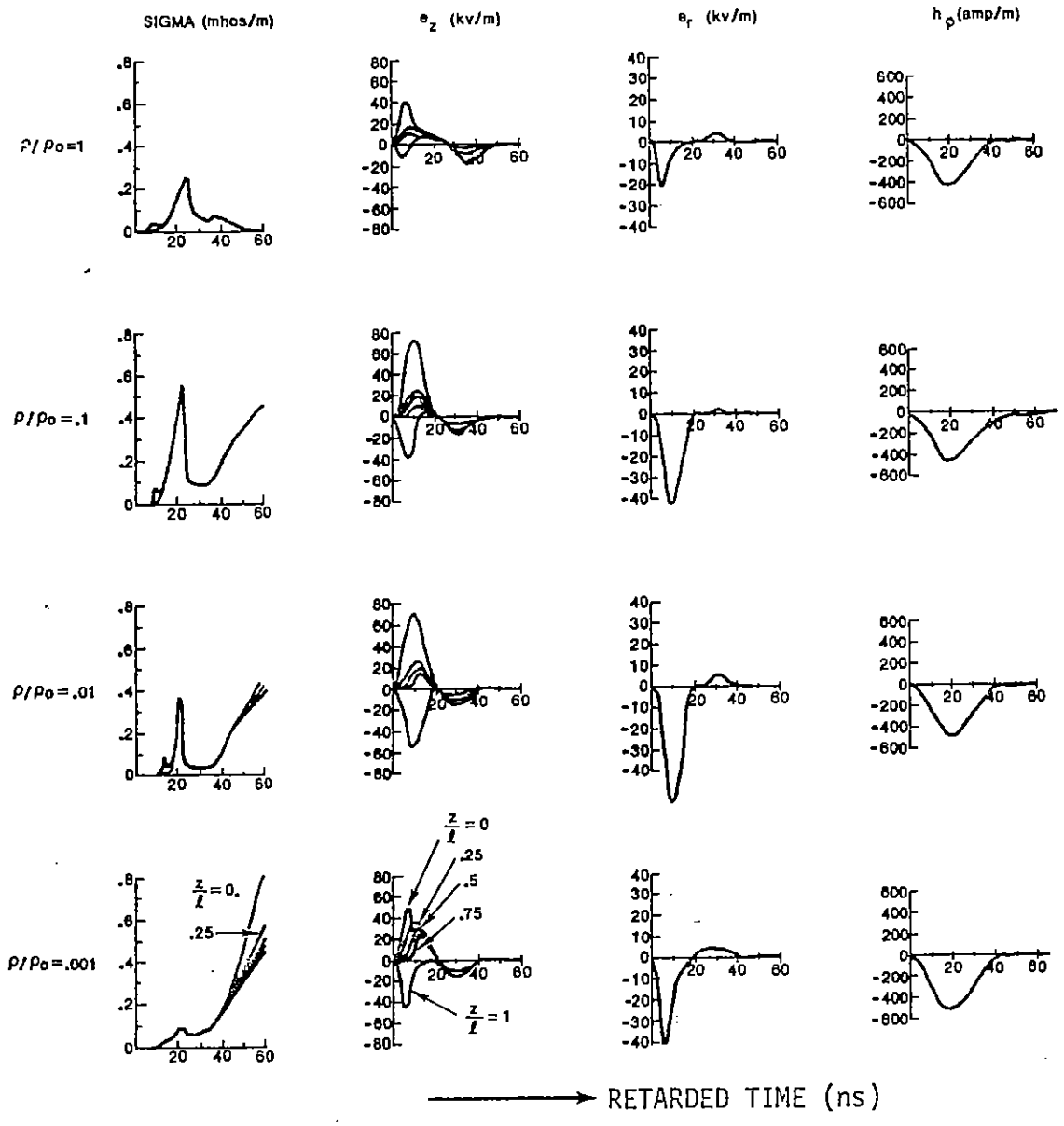

Figure 6. Conductivity and electromagnetic fields within a cylindrical cavity (a = 0.5m, ℓ = 2m), driven by a 1×10^{11} roentgen/sec gamma flux, E_γ = 1 MeV.

The basic shape should be that of a doublet, first positive, then negative, of about 40 nsec total duration. The deviations from this shape are caused by the nonlinearities and time dependence of the air conductivity. It should also be noted that the e_z fields are no longer symmetrical about the center of the canister; increased conductivity makes the field more local in nature so they tend to be more similar. In the top three conductivity curves, there are little early time peaks in the conductivity at the far end of the cylinder. When the e_z component of the field passes through zero, there is an abrupt increase in μ_e (Figure 3), reflected directly in σ. Note that for $\rho/\rho_o = .001$, the e_z field never crosses the axis early; no peak occurs until 20 nsec, when all the field components pass through zero. Note also that the increase in σ corresponding to decreases in e_z will make it more difficult to e_z to increase again. This effect tends to spread out the zeros of the pulse.

Further, it may be noted that the maximum field does not occur at either the highest or the lowest relative air density. The increase in secondary electrons as in (28) is not totally offset by the decrease in mobility (Figure 4) so that the early-time conductivity is a little higher for $\rho/\rho_o = 1$ and the peak fields are a little lower. At the lowest relative air density, "breakdown" occurs at early times (~8 nsec) limiting the fields.

Conclusions

These studies have revealed that the magnetic fields within the air media are not seriously affected by air conductivity, except for a little spreading of the pulse (Figure 6). For the pickup of small loops, simplifying assumptions are valid. For long cable runs within the canister where the electric field, its peak, risetime and distribution are important, the numerical solution provided here should be useful.

Acknowledgment

The authors wish to acknowledge the many helpful conversations with Dr. Conrad Longmire during the preparation of this paper.

References

1. Baum, C. E., "Unsaturated Compton Current and Space Charge Fields in Evacuated Cavities," AFWL Theoretical Note TN-5, 20 January 1965.

2. Mangan, D. L. and G. J. Scrivner, "EMP Response of a Cavity: Field Generation Within a Lossy Dielectric Cylinder Excited by a Radiation Pulse," IEEE Trans. Nuc. Sci., vol. NS-19, 1972, p. 41 (also) AFWL Theoretical Note 168.

3. Scrivner, G. J. and D. L. Mangan, "On the Adequacy of a Straightforward Perturbation Expansion for Estimating the Electromagnetic Response Within a Lossy Dielectric Cylinder Excited by a Radiation Pulse," IEEE Trans. Nuc. Sci., vol. NS-20, 1973, p. 108 (also) AFWL Theoretical Note 173.

4. Yee, K. S., "Numerical Solution of Initial Boundary Value Problems Involving Maxwell's Equations in Isotropic Media," IEEE Trans. Ant. Prop. , vol. AP-14, May 1966, pp. 302-207.

5. Taylor, C. D., D. H. Lam, and T. H. Shumpert, "Electromagnetic Pulse Scattering in Time-Varying Inhomogeneous Media," IEEE Trans. Ant. Prop., vol. AP-17, September 1969, pp. 585-589 (also) AFWL Interaction Note 41.

6. Karzas, W. J. and R. Latter, "Detection of the Electromagnetic Radiation From Nuclear Explosions in Space," (Rand Corporation), AFWL Electromagnetic Pulse Theoretical Note 40, October 1964.

7. Longmire, C. L., "Theory of the EMP from Nuclear Surface Bursts," Los Alamos Nuclear Corporation, LANC-R-8, January 1970.

8. Longley, H. J. and C. L. Longmire, "Development of the CHAP EMP Code," Mission Research Corporation, MRC-R-3, January 1972 (C).